2．「$Al_xGa_{1-x}N$の光学的特性と GaN MSM UV検出器」

CHAPTER 1
General Introduction

1. 1 BACKGROUND

1.1.1 Ultraviolet radiation

Adjacent to and just beyond visible light in the spectrum is the ultraviolet region, discovered by johann wilhelm Ritter (1776~1810). Photon energies therein range from roughly 3.1 eV to 124 eV. UV radiations from the Sun will thus have more than enough energy to ionize atoms in the upper atmosphere and in so doing create the ionosphere. These photon energies are also of the order of the magnitude of many chemical reactions, and ultraviolet radiations become important in triggering those reactions. UV radiation of $200<\lambda<300$ nm is absorbed by the ozone (O_3) layer enveloping the earth, and the UV radiation of 110 nm$<\lambda<$250 nm is absorbed by molecular oxygen, both of which for the terrestrial atmosphere. UV radiation with $\lambda<110$ nm is absorbed essentially by all types of atomic and molecular gases of the atmosphere rendering it non-existent on the surface of the earth. These are the reasons why UV region with $\lambda<$ 200 nm is generally called the vacuum UV region. The spectral region between 250 and 300 nm is of particular interest. The ozone present at 15 to 20 km altitude absorbs the incident solar radiation for wavelengths smaller than 300 nm. As a consequence, any radiation emitted on earth or at low altitude between 250 and 300 nm can be easily observed due to the absence of background radiation under the condition that the detector does not see the background radiations above 300 nm. Such detectors are called solar blind.

Conventionally, the UV spectrum is divided into a number of sub-UV regions:[1]

near ultraviolet	NUV	400–300 nm (3.1–4.1 eV),
mid ultraviolet	MUV	300–200 nm (4.1–6.2 eV),
far ultraviolet	FUV	200–100 nm (6.2–12.4 eV),
extreme ultraviolet	EUV	100–10 nm (12.4–124 eV).

In addition, the following names for UV regions are also often mentioned:

vacuum ultraviolet	VUV	200–10 nm (6.2–12.4 eV),
deep ultraviolet	DUV	350–190 nm (3.5–6.5 eV),
ultraviolet-A	UV-A	400–320 nm (3.1–3.9 eV),
ultraviolet-B	UV-B	320–280 nm (3.9–4.4 eV).

1.1.2 Ultraviolet detectors

In general, UV detectors may be categorized as photon detectors (photodetectors) and thermal detectors (Fig. 1.1).

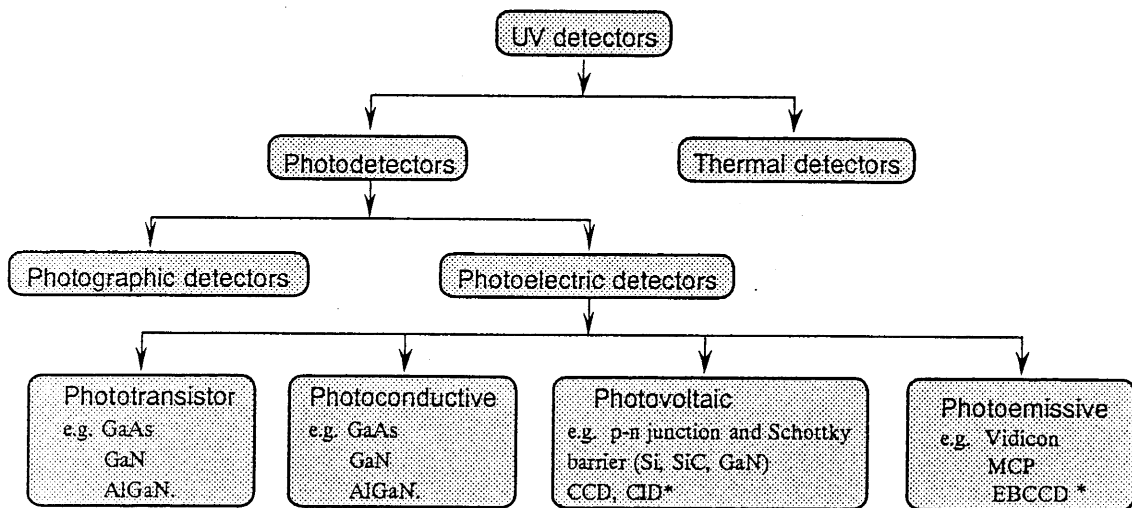

*CCD--charge couple devices,MCP--microchannel array plates.

FIG. 1.1. Classification of ultraviolet detectors (after Ref.1).

The photodetectors are highly sensitive to radiation and used very widely to ensure the rate of photon arrival. Photon detection is through absorption and ensuing creation of free electrons and holes, which lead to a current flow in the material. The change in electronic energy distribution resulting from this absorption of photons gives rise to an observed electrical signal. If they are designed appropriately in a suitable material, they could respond only to UV radiation of certain selected wavelengths.

UV photodetectors have traditionally been devoted into two distinct classes, namely,

photographic and photoelectric. The photoelectric detectors are known to yield a greater stability of response and a greater linearity characteristics. This is achieved by a considerable recent progress in image recording and processing as evidenced by the recently developed photovoltaic (PV) and photoemissive array detectors. Interestingly, these two detectors can offer, for the first time, the sensitivity and radiometric stability of photomultipliers, which paves the way to a high-resolution image capability.

In the photoemissive UV detectors, the photons are incident on the solid surface realizing photoelectron into the vacuum providing that the barrier to electron emission is eliminated preferably by a surface treatment. Applying a voltage between the photocathode surface and a positively biased anode causes a photoelectron current to flow in proportion to the intensity of the incident radiation. As the surface material plays a key role in the functioning of this type detector, the wavelength range of sensitivity is dictated primarily by the absorption band of the cathode arterial and to some extent the work function of its surface. In the semiconductor detectors, the photons are absorbed in the bulk of the semiconductor material producing electron-hole pairs which are separated by an electrical field. These detectors make use of the internal photoelectric effect where the energy of the photons is large enough to scatter the electrons from valence band into the conduction band of the semiconductor material. Applying a voltage across the absorbing region causes a current to flow in proportion to the intensity of the incident radiation.

The most common UV photodetectors currently in use today are the photomultiplier tube (PMT) and the UV-enhanced Si photodetector. Due to its well-established technology, silicon is the semiconductor usually used for photodiodes, although commercial GaAs and GaAsP based photodiodes are also available. The UV-enhanced Si photodetector is typically a *p-i-n* diode with a special antireflection coating designed UV wavelengths, a Schottky barrier photodetector, or an inversion layer photodiode. All three device structures have the advantage that they can be fabricated in a very mature material using a conventional device structure. Since they are all semiconductor photodetectors, they can be made by very small and highly reliable. They also can

be integrated with conventional VLSI components. Although the UV-enhanced Si photodiode has some very important advantages, it does not have very high speed compared to longer-wavelength Si photodetectors, the currents are high (typically in the nanoampere range), and quantum efficiency is poor. For operation in the deep UV, Si photodiodes may suffer reduced quantum efficiency due to a degradation of the SiO_2/Si interface after prolonged UV exposure. In addition, UV-enhanced Si photodetector are not solar-blind devices.

As a kind of photoelectric UV detectors, PMTs are extremely sensitive UV photodetectors that are capable of achieving, through internal gain, responsivities of >600 A/W [2]. PMTs also have high speed and low dark current. A PMT operates by first collecting photons on a cathode that is constructed of an appropriate photoemissive material. The work function of this material is chosen such that photons with energies of interest cause electrons to be emitted from the cathode surface. The cathode is held at very high negative potential relative to the current collecting anode. Between the cathode and anode are a series of dynodes that are held at positive potential relative to the cathode. Emitted electrons are accelerated through the field and into the dynode surface where the secondary emission of electrons occurs. This process is repeated for each dynode, resulting in potentially very large gain ($>10^6$). All electrons are collected at the anode, where a photocurrent is registered. The dark current of a dynode PMT is typically extremely small (<0.1 fA).

Although PMTs are very effective, they are bulky and require very high voltages to operate (usually > 1kV). In addition, the PMT is fragile device that is not suited for many military or space application. Like the Si photodetector, it is also not solar-blind. Costly filters must be used to attenuate unwanted visible and IR radiation with the associated insertion loss. Thus , there is the need for a high-performance, solid-state, solar-blind ultraviolet photodetector that can be cost-effectively manufactured into high-density arrays. One possible candidate for the construction of such a device is the direct-bandgap semiconductor alloy, aluminum gallium nitride ($Al_xGa_{1-x}N$).

1 . 1. 3 GaN-based material system solution

Gallium nitride is a wide-bandgap semiconductor that has received renewed interest based on recent advances in crystal growth and optoelectronic device fabrication.[3] Both *n*-type and *p*-type doping GaN have become routine, although much work still needs to be done to understand dopant activation in *p*-type materials.[4] It is now well understood how to fabricate good *n*-type ohmic contacts and reasonable *p*-type contacts. Heterostructures comprised of the ternary alloys InGaN and AlGaN are now commonplace. To date, most of the interest in GaN, and the alloys in the $Al_xIn_yGa_{1-x}N$ system, has been for light emitters (e.g., LED's [5-8] and laser diodes [9]). There is also significant research underway in the area of GaN-based high-temperature, high-power electronics and microwave devices.[10,11] Recently, interest has grown in using this material system to fabricate UV photodetectors.[12]

Table 1.1. Basic parameters of semiconductors used in UV photodetector (300K).

	Si	GaAs	GaP	GaN	AlN
Energy gap (eV)	1.12	1.43	2.26	3.45	6.2
Energy of direct band (eV)	3.4	—	2.78	—	—
Breakdown field ($V\,cm^{-1}$)	3×10^5	4×10^5	1×10^6	2.6×10^6	2×10^6
Electron mobility ($cm^2\,V^{-1}\,s^{-1}$)	1400	8500	250	900	300
Hole mobility ($cm^2 V^{-1}\,s^{-1}$)	450	400	150	150	14
Radiation recombination coefficient ($cm^3\,s^{-1}$)	10^{-14}	7×10^6	10^{-13}		4×10^{11}
Density ($g\,cm^{-3}$)	2.33	5.32	4.14		3.23
Lattice constant (Å)	5.431	5.653	5.45	3.19	3.11
				5.19	4.98
Electron affinity (eV)	4.05	4.07	3.08		0.6
Dielectric constant, static	11.7	12.9	11.1	9.5	8.5
Melting point (℃)	1412	1240	1457		3000
Thermal conductivity ($W\,cm^{-1}\,K^{-1}$)	1.3	0.55	1.1	1.3	3.19
Saturation electron drift velocity ($cm\,s^{-1}$)	10^7	2×10^7	1.25×10^6	2.7×10^7	
Maximum operating temperature (℃)	600?	760?	1250?		

The $Al_xGa_{1-x}N$ material system, spanning band gaps of 3.4–6.2 eV, is ideal for fabrication of solar-blind UV detectors. By varying the Al content, the responsivity cut-off wavelength can be varied from 365 to 200 nm. Since the quantum efficiencies are high due to the direct gap of the Ga-rich alloys, there is the ability to form heterojunctions and high temperature operation is

possible. SiC *p-n* junction photodiodes are also operable at high temperatures, but they lack the other advantages of AlGaN devices. Specifically, GaN-based photodetectors could be fabricated into two-dimesional arrays that are suitable for UV sensor and multispectral imaging systems. If properly constructed, GaN-based photodetectors could offer significant advantages over PMT detectors in terms of size, cost, robustness, complexity, bandwidth, and solar-blind operation. As comparison, the basic parameters for UV photodetector fabrication in Si, GaAs, GaP, GaN, and AlN are listed in Table 1.1.[13]

The applications for the nitride devices include:

* Biological and chemical sensors: ozone, pollutants and other chemical and biological agents.

* Flame sensors: fire alarms, missile plume detection, combustion control.

* Optical communications: secure space-to-space transmission.

* UV-emitter calibration: instrumentation, solar UV monitoring, astronomical studies.

In general, ideal photodetectors require high responsivity, high response speed, minimum noise and high spectral selectivity. In addition, the photodetectors should be compact in size, use low biasing voltages or current, and be reliable under operating conditions. The importance and priority of these specifications depend on the application field. When used as UV photodetectors in jet engines, automobiles, and furnaces (boilers), the devices would allow optimal fuel efficiency and control of effluents for a cleaner environment. To a limited extent, visible-blind GaN photodetectors are in commercial use today. Several companies sell GaN photodiodes that are used for flame detection against a warm background (such as detect pilot lights and burner flames inside large industrial furnaces). Some large optics distributors now carry GaN-based device for general-purpose UV detection requirements. For this application, a visible-blind GaN photodetector with high responsivity is generally sufficient.

The biological action of the solar UV radiation has a strong dependence on the wavelength, and depends on the specific biological process being studied (erythema or skin sunburning, DNA damage, plant damage, germicidal effects, bacteria killing and skin cancer, etc.). Because of its

practical importance for human beings, the erythema (skin sunburning) action has been extensively studied. Such response is the most widely uesed UV biological action response, and is presently achieved by using low band gap photodiodes (Si, GaAs, GaAsP) and a series of filters and phosphor coatings. By proper detector design, the erythema weight action is approximated by single AlGaN photodiode without any filter. The skin cancer response can be obtained by using an AlGaN (UV-B region) photodiode and an InGaN (UV-A region, 400–320 nm) diode.[14]

Military applications, on the other hand, center around missile and aircraft detection, in which case very high sensitivity, low dark current, high speed, and solar-blind operation are all necessitated. The alloy AlGaN with about 50-60 % AlN absorbs in the region of the spectrum where the Sun's radiation is absorbed by the Earth's ozone layer, thereby providing a dark background. An AlGaN UV photodetector operating in this region sees a background that results in reduced radiation noise and allows the detection of minute emission from certain targets. To detect and warn against ground-to-air, air-to-air, air-to-ground, and ground-to-ground missile threats. successfully requires early detection of the missile launch. One promising method of detecting incoming missiles is sensing the UV emissions from the rocket plume. Particularly at altitudes lower than 20,000 ft, the solar-blind region is ideal for this purpose because the solar background radiation is almost entirely absorbed by atmospheric ozone. Thus, the ~3000 K blackbody emission from a missile plume stands out prominently against a dark background, thereby making false alarm rates very low. Such a missile threat warning system, therefore, requires two-dimensional arrays of highly sensitive photodetectors to image the solar-blind UV spectral range. Currently, however, no solid state UV photodetectors have the sensitivity required for this application. For atmospheric detection, one must achieve very high quantum efficiency and very low noise, since the signatures of these potential targets are known to be very weak, and UV propagation in the atmosphere is poor due to Raleigh scattering at the shorter wavelengths. Therefore, there is a need to develop advanced solar-blind heterostructure photodetectors using epitaxial layers of Al_xGa1-_xN to achieve high quantum efficiency, low dark current, and high speed.

The photoconductive properties of GaN were studied by Pankove and in 1974,[15] and the first GaN UV photodetector was reported in 1992[16]. Since then, a number of research teams have developed GaN-based photoconductive,[17] p-n junction,[18] p-i-n device,[19,20] MSM structure,[21] Schottky barrier photodetectors.[22] More recently, the above structures, and phototransistors detectors based on AlGaN has been reported. Figure 1.2. shows a schematic representation of different types of $Al_xGa_{1-x}N$ photodetectors reported in literature. *N*-type material is generally used because of its higher carrier mobility.

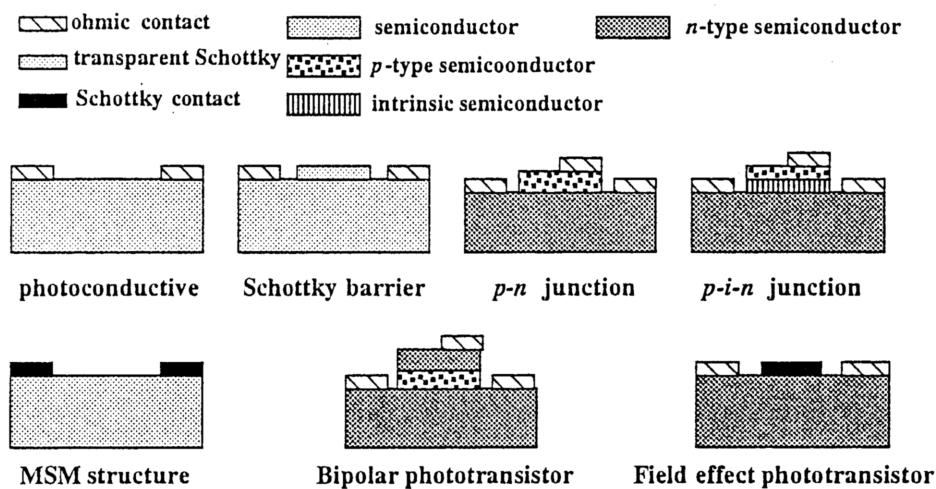

FIG. 1.2. Schematic structure of the different types of $Al_xGa_{1-x}N$ photodetectors.

Table 1.2. presents a collage of various UV photodetectors for comparing and appraising the current state-of-the-art performance. Despite the remarkable developments mentioned above, true solar-blind detectors with very low noise levels and signal amplification have not yet been reported. The ternary AlGaN large AlN mole fractions would have to be prepared high quality. If *p-n* junction varieties are to be used, *p*-doping in such a high mole fraction AlGaN is no easy and none has been demonstrated. These difficulties should, however, be viewed as challenges rather than obstacles as has been the case for just about any advancement. A reasonable midway set of performance goals would be to achieve near 80% to 90% internal efficiency, 10^{-14} W NEP, higher than 100 MHz frequency response, 260 to 290 nm wavelength response, and 10^{-4} of peak response relative response at 300 nm for AlGaN detectors.

Table 1.2. - Comparison of the Performance (Responsivity, R, Internal Gain-Quantum Efficiency Product, G η, NEP, and Photocurrent Decay Time, t) of some State-of-the-Art III-Nitride Photo-detectors.

Detector	Responsivity (A/W)	G η (internal)	Spectral range (nm)	UV-visible ratio	NEP (W)	Response time (s)	Ref.
GaN PC	125	600			>20×10^{-9}		17
$Al_xGa_{1-x}N$ PC	18-300	64-1500	200~240-350			$1\text{-}2\times10^{-3}$	23
GaN MSM-PD	0.15		300~365	~10^3-10^4		23×10^{-12}	21
AlGaN MSM-PD	0.107		250~280	~10^3	3.8×10^{-12}		26
n-GaN Schottky	0.18		200~365		$<4\times10^{-9}$	120×10^{-9}	22
n-AlGaN Schottky	0.07		250~290		6.6×10^{-9}	1.6×10^{-6}	27
GaN *p-n* PD	0.14				7×10^{-14}	1.7×10^{-8}	18
AlGaN/GaN *p-n* PD	0.5					10	24
GaN *p-i-n* PD	0.11	0.48	250~365	~10^3		8.2×10^{-6}	19
GaN *p-i-n* PD	0.10		300~365	~10^3		9×10^{-11}	20
AlGaN/GaN *p-i-n* PD	0.15	0.63	260~365	~10^3	8×10^{-12}	12×10^{-8}	25
GaN *p-π-n* PD	0.14		200~365	~10^3	6.6×10^{-15}	~10×10^{-9}	28
GaN/AlGaN phototransistor	5×10^4	1.7×10^3	200~365	10^8			29
PMT-based imager	~670	~3000			~10^{-15}	<10^{-3}	30

*Limited by measurement setup. The total NEP value at a reverse bias of 28 V is 2.06×10^{-3} W.
PC- -photoconductor, MSM- -Metal Semiconductor metal, PD- -photodiode, PMT- -photomultier.

1. 2 ORGANIZATION OF DISSERTATION

The subject of this work is of interest both in the fundamental and applied fields of $Al_xGa_{1-x}N$ material system. The final goal of our researches is to fabricate high performance $Al_xGa_{1-x}N$ UV photodetectors. In order to achieve this objective, the research works were performed in two steps. The first step conducted investigations on the optical properties of GaN and its ternary alloys $Al_xGa_{1-x}N$. The optical absorption in undoped and Si-doped n-type GaN, which is of great interest in understanding and characterizing the GaN photodetectors, was investigated. Subsequently, a method by using the reflectance measurement was proposed to determine the composition dependence of the bandgap energy (E_g) and bowing parameter of $Al_xGa_{1-x}N$ alloys. As the second step, the fabrication and characterization were performed on GaN MSM-PDs. Consequently, this dissertation presents a synthesis of the above research results and summarized as follows:

The present chapter, as an introduction of this dissertation, reviews the historical development of the UV detector. The applications of the GaN-based UV photodetectors are also introduced. For

these applications, the technical requirements, the state of the art and the remaining open issues are indicated.

Our research works on GaN-based UV photodetector are concentrated on the photovoltaic metal-semiconductor photodiodes and mainly on the MSM structure photodiodes. In Chapter 2, the basic operating principles of the MS photodetectors (Schottky barrier photodiode and Schottky MSM-PD) are presented. Generally the behavior of these devices arises from the interaction between UV radiation and the electrons in the semiconductor GaN, i.e., results from the absorption of UV radiation with consequent electronic effect. The topics are thus introduced from the the optical absorption process in undoped and Si-doped n-type GaN. The following discussions on the photoresponse mechanism show that the optical parameter of interest is the absorption coefficient, $\alpha(\lambda)$, and the electrical parameters of interest are minority carrier diffusivity, D, and diffusion length, L . The chapter also includes a discussion of the performance figures and their analysis method, which can be utilized in understanding the operation of devices and the optimization of performance.

In UV detect application, a crucial property of the $Al_xGa_{1-x}N$ (x=0~1) alloys is the composition dependence of the band gap energy (E_g), which is described by a linear behavior of Al mole fraction (x) and a nonlinear deviation of bowing parameter (b). In chapter 3, a method which utilizes the reflectance measurement to determine E_g and b is introduced.

A fundamental characteristic of great importance in UV photodetector performance is the dark current and photoresponse. For MSM structure photodetector, however, a main problem is the relatively low responsivity due to the shadowing of the interdigitated electrodes. In chapter 4, the fabrication and the characteristics of the back illuminated MSM-PD with the object for improving the UV responsivity are described. The reason for high internal gain is also discussed.

Chapter 5 introduces a novel structure GaN UV MSM-PD with recessed electrodes. Topics therein include the fabrication procedure and the characteristics of this UV photodetector and the mechanism for the improvement of the responsivity.

Finally, in chapter 6, the research works contributing to this dissertation are summarized. The possible limitations, promising developments and future trends of $Al_xGa_{1-x}N$ based photodetectors are addressed.

References

[1] M. Razeghi and A. Rogalski, J. Appl. Phys. **79**, 7433-7473 (1996).

[2] H. Morkoç, IEEE J.Selected Topics in Quantum Elec. **4**, 537 (1998).

[3] S.N. Mohammad, A. Salvador, and H. Morkoç, "Emerging GaN Based Devices," Proc. IEEE **83**, 1306 (1995).

[4] S. J. Pearton, J. C. Zolper, R. J. Shul, and F. Ren, J. Appl. Phys. **86**, 1 (1999).

[5] H. Amano, M. Kito, K. Hiramatsu, and I. Akasaki, Jpn. J. Appl. Phys. **28**, L2112 (1989); I. Akasaki, H. Amano, M. Kito, and K. Hiramatsu, J. Lumin. **48/49**, 666 (1991).

[6] S. Nakamura, T. Mukai, and M. Senoh, Jpn. J. Appl. Phys. **30**, L1998 (1991); Appl. Phys. Lett. **62**, 2390 (1993); **64**, 1687 (1994).

[7] B. Goldenberg, J. D. Zook, and R. Ulmer, Appl. Phys. Lett. **62**, 381 (1993).

[8] R. J. Molnar, R. Singh, and T. D. Moustakas, Appl. Phys. Lett. **66**, 268 (1995).

[9] S. Nakamura, M. Senoh, S. Nagahama, N. Iwasa, T. Yamada, T. Matsushita, H. Kiyoku, and Y. Sugimoto, Jpn. J. Appl. Phys. **35**, L74 (1996).

[10] M. Asif Khan, M. S. Shur, J. N. Kuznia, Q. Chen, J. Burm, and W. Schaff, Appl. Phys. Lett. **66**, 1083 (1995); S.T. Sheppard, K. Doverspike, W.L. Pribble, S.T. Allen, J.W. Palmour, L.T. Kehias, T.J. Jenkins, IEEE Electron. Dev. Lett. **20**, 161(1999).

[11] J.I. Pankove, S.S. Chang, H.C. Lee, R.J. Molnar, T.D. Moustakas, and B. Van Zeghbroeck, IEDM **94**, 389; J.I. Pankove, M. Leksono, S.S. Chang, C. Walker, B. Van Zeghbroeck, MRS Internet J. Nitride Semicond. Res. **1**, 39 (1996).

[12] M. P. Ulmer, M. Razeghi, and E. Bigan, Proc. SPIE **2397**, 210 (1995).

[13] S. J. Pearton, F. Ren, A. P. Zhang and K. P. Lee, Mater. Sci. Engng. **R 30**, 55 (2000).

[14] J.-Y. Duboz, Phys. Stat. Sol. (A) **176**, 5 (1999).

[15] J.I. Pankove and J.E.Berkeyheiser, J. Appl. Phys. **47**, 3892 (1974); J. I. Pankove and H. E. P. Schade, Appl. Phys. Lett. **25**, 53 (1974).

[16] M. A. Khan, J. N. Kuznia, D. T. Olson, J. M. Van Hove, M. Blasingame, and L. F. Reitz, Appl. Phys. Lett. **60**, 2917 (1992).

[17] M. Misra, D. Korakakis, R. Singh, A. Sampath, and T.D. Moustakas, Mater. Res. Soc. Proc. **449**, 597 (1997).

[18] Q. Chen, M. Asif Khan, C.J. Sun, and J.W. Yang, Electron. Lett. **31**, 1781 (1995).

[19] J.M. Van Hove, R. Hickman, J.J. Klaassen, and P.P. Chow, Appl. Phys. Lett. **70**, 2282 (1997).

[20] J.C. Carrano, T. Li, D.L. Brown, P.A. Grudowski, C.J. Eiting, D. Lambert, J.D. Schaub, R.D. Dupuis, and J.C. Campbell, Electron. Lett. **34**, 692 (1998); J.C. Carrano, T. Li, D.L. Brown, P.A. Grudowski, C.J. Eiting, R.D. Dupuis, and J.C. Campbell, Electron. Lett. **34**, 1779 (1998).

[21] J.C. Carrano, T. Li, P.A. Grudowski, C.J. Eiting, R.D. Dupuis, and J.C. Campbell, J. Appl. Phys. **83**, 6148 (1998); J.C. Carrano, T. Li, D.L. Brown, P.A. Grudowski, C.J. Eiting, R.D. Dupuis, and J.C. Campbell, Appl. Phys. Lett. **73**, 2405 (1998).

[22] Q. Chen, J.W. Yang, A. Osinsky, S. Gangopadhyay, B. Lim, M.Z. Anwar, M. Asif Khan, D. Kuksenkov, and H. Temkin, Appl. Phys. Lett. **70**, 2277 (1997).

[23] B.W. Lim, Q.C. Chen, J.Y. Yang, and M. Asif Khan, Appl. Phys. Lett. **68**, 3761 (1996).

[24] Honeywell, Inc., unpublished results, private communications with D. Zook and B. Goldenberg.

[25] G.Y. Xu, A. Salvador, W. Kim, Z. Fan, C. Lu, H. Tang, H. Morkoç, G. Smith, M. Estes, B. Goldenberg, W. Yang, and S. Krishnankutty, Appl. Phys.Lett. **71**, 2154 (1997).

[26] T. Li, D.J.H. Lambert, A.L. Beck, C.J. Collins, B. Yang, M.M. Wong, U. Chowdhury, R.D. Dupuis, and J.C. Campbell, Electron. Lett. **36**, 1581 (2000).

[27] A. Osinsky, S. Gangopadhyay, B.W. Lim, M.Z. Anwar, M. A. Khan, D. Kuksenkov, and H. Temkin, Appl. Phys. Lett. **72**, 742 (1997).

[28] A. Osinsky, S. Gangopahyay, R. Gaska, B. Williams, M.A. Khan, D. Kuksenkov, and H.

Temkin, Appl. Phys. Lett. **71**, 2334 (1997).

[29] W. Yang, T. Nohava, S. Krishnankutty, R.Torreano, S. McPherson, and H. Marsh, Appl. Phys. Lett. **73**, 978 (1998).

[30] Lockheed-Martin, PMT-based imager; Air Force Research Laboratory (1997).

CHAPTER 2
UV Semiconductor Photodetectors: Basic Operating Principles and Performance Characteristics

2. 1 INTRODUCTION

The fundamental purpose of any photonic detector is to convert incident optical radiation into an electrical signal which can be amplified, displayed and/or retransmitted. Principally, semiconductor photodetectors are light-weight, compact, typically operate at relatively low applied voltages and are generally low in cost. For these reasons, semiconductor photonic detectors are attractive in many detection systems. Typically, semiconductor photodetectors are employed in one of two applications, either in imaging or lightwave communications. The choice of application greatly affects the performance criterion of the detector. For imaging applications, the key issues by which a detector is judged are its signal to noise ratio; spatial resolution, gray scale resolution (the ability to discriminate between different shades on a totally white to totally black contrast scale); ability to operate through a range of high to low input light levels, and spectral response. Detectors employed in modern lightwave communications systems have very different performance requirements. In this application, the detector must be designed to ensure signal recognition, avoid inter symbol interference, and operate at high speeds or bandwidths. The speed of response of the detector in lightwave communications systems is crucial to its performance. In contrast, in most imaging applications, speed of response is relatively unimportant. Therefore, the design and performance criterion of a photonic detector depends critically upon its planned application.

There are several important classes of semiconductor based photonic detectors. Semiconductor photodetectors can be classified into five general categories. These are photoconductors, *p-n* junctions, Schottky barrier diodes, phototransistors, and metal-insulator-semiconductor (MIS) devices. Of these device types, only photoconductors, photodiodes and phototransistors can readily

supply gain. Detector gain is used to overcome the noise floor of the following electronics. This is particularly important in high frequency applications, such as lightwave communications systems, where the noise floor of the electronics is relatively high. Each of the detector types which supply gain offers specific advantages and disadvantages. Phototransistors are attractive for detection applications since they can achieve high gain through transistor action, but they are relatively more complicated to fabricate and generally require sizable chip area. Photoconductors are inherently simple devices that operate at low voltages and are completely compatible with planar integrated circuit technologies. However, these devices are fundamentally limited in gain-bandwidth performance. Nevertheless, the simplicity afforded by a metal-semiconductor-metal (MSM) design makes these devices highly attractive in on-chip detector applications. Photodiodes, especially avalanche photodiodes, can potentially provide higher gain-bandwidth performance than photoconductors, require less chip area and fabrication complexity than phototransistors and can operate at high gain and low noise.

Owing to the above mentioned inherent advantages, MSM structures and avalanche photodiodes are arguably the most promising semiconductor photonic based structures for communications and on-chip detection. Both device types offer high bandwidth operation, wide spectral coverage, gain mechanisms, high responsivity and compatibility with integrated circuit fabrication technology. The gain, bandwidth and responsivity of MSM and photodiode detectors are highly sensitive to the individual device designs. Variations in the device geometry, applied bias, doping concentrations, etc., can greatly influence the device performance. The degree to which these variations alter the device performance, or its sensitivity, must be characterized to ensure reliable performance.

In this chapter, we will first present the basic operating principles of Schottky barrier and MSM structure photodiodes, and then discuss the main parameters of their performance characteristics to figure out the optimal design for each structure. Only the metal-semiconductor photodetector will be concerned in this chapter and mainly the MSM structure photodetector.

2. 2 BASIC OPERATING PRINCIPLES

2.2.1 Optical Absorption in direct wide bandgap semiconductor--GaN

In order for a semiconductor device to be useful as a photodetector, some property of the device should be affected by radiation. The most commonly used property is that the conversion of incident irradiation into electron-hole pairs which can be detected in a properly chosen electric circuit.

Gallium nitride (GaN) is one of the direct wide gap semiconductors. It crystallizes in the wurtzite (WZ) structure. The valence bands consist of A, B, and C bands, which are split even at the G point due to the crystal field and spin-orbit interaction. Therefore, the corresponding exciton structure consists of A, B, and C excitons as the first approximation (Fig. 2.1). Due to the large exciton binding energy (27 ± 1 meV) [1, 2] of GaN, which is larger than the thermal energy of electrons at room temperature (26 meV), the optical properties of GaN are mainly determined by excitons even at room temperature.

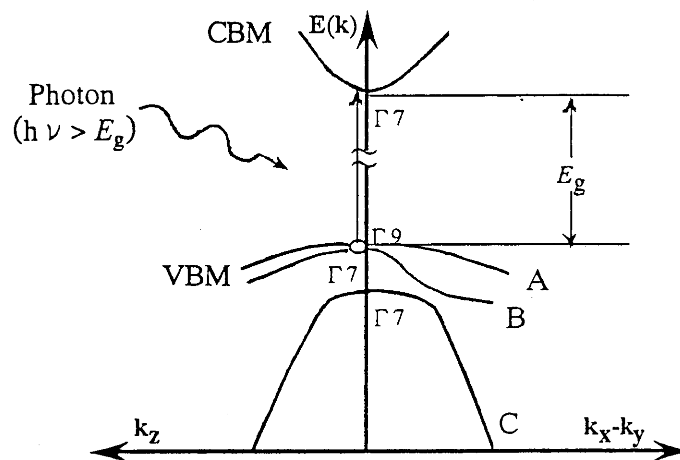

Fig. 2.1. Schematic band structure around the Γ point of WZ GaN. The energy dispersions along k_z direction and in k_x-k_y plane are shown. At k=0, the top of the valence band is split by crystal field and spin orbit coupling into the A(Γ9), B(Γ7), and C(Γ7) states. After [3, 4].

When incident irradiation impinges on a semiconductor, it can scatter an electron in the valence band into the conduction band. This process, called absorption of a photon. In order to take the

electron from fully occupied valence band to the empty conduction band, the photon energy must be at least equal to the bandgap of the semiconductors. The photon absorption process is strongest when the photon can directly cause an electron in the valence band to go into the conduction band. Since the photon momentum is extremely small on the scale of the electron momentum, the conservation of momentum requires that the electron-hole transitions are vertical in k-space, as shown in Fig. 2.1. Such transitions are only possible near the bandedge for direct bandgap semiconductors, such as GaN. For such semiconductors one can write the absorption coefficient as

$$\alpha(\hbar\omega) = \frac{2\pi q^2\hbar}{3n_r c m_0^2 \varepsilon_0} \frac{|p_{cv}|}{\hbar\omega} \frac{\sqrt{2}(m_r^*)^{3/2}(\hbar\omega - E_g)^{1/2}}{\pi^2\hbar^3}, \tag{2. 1}$$

where m_r* is the reduced e-h mass, n_r is the refractive index, $\hbar\omega$ the photon energy, E_g the bandgap and p_{cv} is a momentum matrix element which allows the transition to take place. For direct gap semiconductor GaN, when the various values for the constants are plugged into Eq. (2.1), the absorption turns out be $\hbar\omega$, E_g in eV

$$\alpha(\hbar\omega) \cong 4\times10^6 \left(\frac{m_r^*}{m_0}\right)^{3/2} \frac{(\hbar\omega - E_g)^{1/2}}{\hbar\omega} cm^{-1}. \tag{2. 2}$$

As can be seen from Eq. (2.2), the absorption is zero above a cutoff wavelength given by λ_c, which can be expressed as

$$\lambda_c = \frac{hc}{E_g} = \frac{1.24}{E_g(eV)}, \quad (\mu m) \tag{2. 3}$$

where E_g is the semiconductor bandgap. It should be noted that the electron-hole interaction produces excitons which modify the optical spectra near the bandgap. Thus, optical absorption can occur a few meV (for GaN is about 27.5 meV) below the bandgap. Moreover, it has been observed by many researchers that the intrinsic absorption edge is not as steep as suggested by Eq. (2.1). For GaAs, GaN, and other direct gap materials, the absorption edge is blunted (Moss and Hawkins 1962; Sturge 1962; Hill 1964). Urbach (1953) commented that the absorption coefficients in many non-metallic solids tend to have an exponentially sloping edge expressed as

$$\alpha = \alpha_0 \exp[A(\hbar\omega - B)], \quad (2.4)$$

for the major steep region. However, the exponential steepness of increases as one proceeds towards the top of the edge. The characteristics become more prominent at lower temperature.

The explanation for the Urbach edge was first given by Redfield (1963). He suggested that in the sample there may be doping inhomogeneities and also internal strains. These give rise to a microscopic electric field in the sample. Franz (1958) and Keldysh (1958) independently established that an electric field produces absorption tails in a semiconductor. Redfield argued that the intrinsic slope variation arises from the Franz-Keldysh effect caused by variations in the microscopic electric field.

On the other hand, it was found that the exponential absorption edge is correlated quite well with transition involving band tails, which can be controlled by doping. When the carrier concentration in a semiconductor is large due to the presence of a large impurity density, the coulomb potential of randomly distributed impurities causes a significant alteration of energy states near the band edge. with increasing impurity concentrations, the hydrogen-like impurity wave functions begin to overlap. As a result the energy levels of the impurities broaden to form a band, known as an impurity band. In addition, an impurity atom introduces a local variation in the potential energy of an electron because of the difference of the nuclear potentials of the impurity and the host atom. This local random variation of the potential energy modifies the position of the band edges. Consequently, the band extend beyond their respective position in the intrinsic material. The extended part of the band is called the *band tail.* A high impurity density also means a high carrier density. The lattice potential which an electron faces is then affected by the presence of other electrons, or in other words the lattice potential is screened. When the electron gas is dense, the wave functions of adjacent electrons overlap and the interaction becomes prominent. The electrons repel one another and the electrons with same spin avoid each other. The behavior of an electron is thus controlled by all other electrons and the effect is known as correlation. The results of the two effects is a lowering of the potential energy for both the electron and hole, which is known as

band-gap shrinkage. [5]

The absorption coefficient for the different n-type Si doping concentration at room temperature is shown in Fig. 2.2.[6] The absorption coefficient of undoped GaN demonstrates two distinct exciton oscillation peaks. The profile of the exciton peaks can still be observed even at carrier concentration as high as 1×10^{18} cm^{-3}, which indicates a large exciton binding energy. The absorption coefficients show a significant decrease around the location of the excitons peaks with increasing doping level, which can be attributed to the quenching of exciton by ionized impurities. Because the ionized carriers screen the Coulomb interaction between electrons and holes, the probability for exciton formation is reduced and the exciton absorption peak is therefore eliminated.

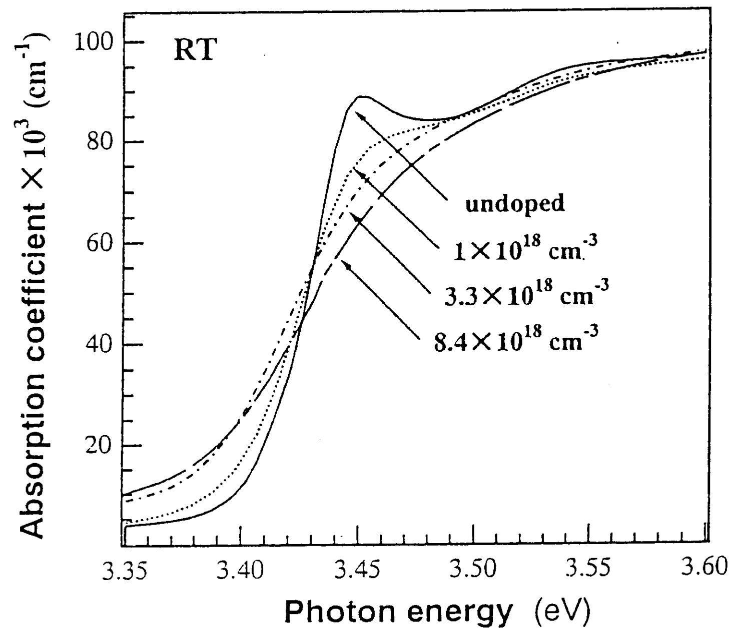

Fig. 2.2. Absorption coefficient of GaN with various carrier concentrations, as a function of photon energy.

Moreover, as the doping concentration increases, the absorption below the band gap increases and the band edge absorption decreases less rapidly compared to that of the undoped GaN. As discussed above, the ionized impurities perturb the bands via the Coulomb interaction, which induces a strong local field and band tailing and thus, changes the slope of the absorption edge. Therefore, both characteristics indicate that band gap narrowing and band tailing effect dominate in

the n-type GaN near band edge optical absorption. For n-type III-V semiconductors such as GaAs and InAs, the band filling effect can usually be observed in the heavily doped case due to the small carrier effective mass. The Fermi level can easily move into the conduction band as the doping concentration increases above the degeneracy limit. As a result, the absorption edge shifts to the higher energy region. The band filling effect is not evidently observed for n-type GaN even at doping concentration as high as 8.4×10^{18} cm^{-3}. The Fermi level is 0.066 eV above the bottom of conduction band at this doping level, and extreme degeneracy is not realized due to the large electron effective mass of GaN.

For GaN, the optical absorption at the bandegdes is strong because the optical absorption can occur without a phonon participation. For detection of an optical signal, the incident light should be absorbed. It is known that radiation absorption actually occurs in the region of finite thickness near the surface, corresponding to the skin depth of the electromagnetic wave penetrating into the surface of matter. If L is the thickness of the semiconductor layer, the fraction of incident light absorbed in it is approximated

$$1-\exp(-\alpha L) \tag{2.5}$$

Thus, for strong absorption, we must have

$$L > 1/\alpha(\hbar\omega) \tag{2.6}$$

The dependence of absorption coefficient on wavelength (absorption coefficient spectrum) is one of most interesting optical properties in characterization and design of semiconductor UV photodetector. Once the absorption coefficient for a semiconductor is known, one then knows the rate at which electron-hole pairs will be generate. The relation between the absorption coefficient and the rate of electron-hole generation will be discussed in the next section.

2.2.2 Schottky-barrier photodiodes

Schottky diodes (surface-barrier diodes) having a metal (M)–semiconductor (S) structure have some features in common with *p–n* structures (the presence of the potential barrier) and differ substantially in the energy diagram (the depletion region where the electric field is high is at the

semiconductor surface and the potential barrier height is substantially lower than the semiconductor bandgap energy), in the mechanism of current flow (it is thermionic emission for Schottky diodes) and in fabrication technology. It appears, therefore, that M–S structures should have higher short-wavelength sensitivity (carrier generation occurs in the depletion region with high built-in electric field) and faster response (the current is due to the transport of majority charge carriers and not the recombination–generation processes); their fabrication technology is simpler but they have lower breakdown voltages, larger leakage currents and lower photovoltage compared with *p–n* structures based on the same semiconductor material.

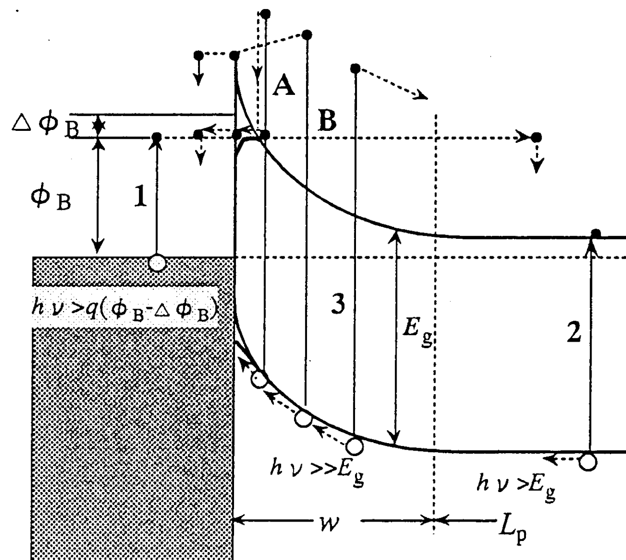

Fig. 2.3. Energy-band diagram of a Schottky-barrier photodetector. The different mechanisms of the photoeffect (1. electron generation in the metal, 2. electron-hole generation in the semiconductor outside the depletion region, 3. electron-hole generation in the semiconductor within the depletion region) and losses (a. electron diffusion or thermionic emission against the contact field, b. electron quasiballistic losses) are shown. Full curves are the energy-band diagram including barrier height decrease due to the Schottky effect.

In front-illuminated Schottky photodiodes, the light that crosses the semitransparent Schottky contact is absorbed in the semiconductor, generating electron-hole pairs. The direction of incident illumination is perpendicular to the plane of the Schottky barrier. Depending on the wavelength of the incident light and the semiconductor used, a certain percentage or all the incident light is

absorbed in the depletion layer of the barrier. The current responsivity of M–S structures (Fig. 2.3.) is determined by the following.

(I) The first process is the generation of electrons in the metal and their injection into the semiconductor at incident photon energies exceeding the barrier height $q\phi_B$ of the metal–semiconductor potential barrier.

(II) The second is the generation of electron–hole pairs in the semiconductor and separation of the pairs by the built-in electric field at $h\nu > E_g$. The photocurrent represents the sum of contributions from charge carriers generated in the depletion region of width w and from carriers that reached this layer from the adjoining region of extent L_p (minority charge carrier diffusion length).

The second process is more efficient than the first and therefore the long-wavelength limit of the photosensitivity spectrum is close to the bandgap value in direct-band semiconductors and to the threshold energy for direct optical transitions in indirect-band semiconductors. At photon energies well in excess of E_g the photosensitivity is observed to drop, although less dramatically than in *p–n* structures. This drop was explained by loss of photogenerated carriers occurring through carrier drift against the built-in field,[7] by thermionic emission,[8] by quasiballistic electron transport [9] or by a drop in the internal quantum yield.[10]

The total current under the illumination is then given by

$$I_{T(ph)} = A\left(J_{drift} + J_{diff} + J_{emis}\right), \tag{2. 7}$$

where A is the Schottky contact area, and J_{drift}, J_{diff}, and J_{emis} are the current densities due to carrier drift, diffusion, and photoemission from the metal, respectively. Recombination and thermal generation of carriers inside the depletion region will be neglected, but may be noticeable in material with a high concentration of recombination centers, and then would cause additional modifications of the Eq. (2.7).

The *drift photocurrent* can be expressed as

$$J_{drift} = -q\int_{DR} G(x)dx \ , \tag{2. 8}$$

where $G(x)$ is the generation rate, given by

$$G(x) = \Phi_{ph} T_m(\lambda)\alpha(\lambda)e^{-\alpha(\lambda)x}. \quad (2.9)$$

being Φ_{ph} the photon flux reaching the device, $T_m(\lambda)$ the transmittance of the semitransparent metal, and $\alpha(\lambda)$ the semiconductor absorption coefficient. The drift current density due to carriers generated inside the depletion region with a width of w is then obtained as

$$J_{drift} = -q\int_0^w G(x)dx = -q\Phi_{ph}T_m(\lambda)\left(1-e^{-\alpha(\lambda)w}\right). \quad (2.10)$$

The *diffusion photocurrent* is given by

$$J_{diff} = -qD_p\left(\frac{\partial p}{\partial x}\right)_{x=w}, \quad (2.11)$$

where D_p is the minority (hole) diffusion constant. The hole concentration, $p(x)$, can be obtained from the continuity equation

$$D_p\frac{\partial^2 p}{\partial x^2} - \frac{p-p_{n0}}{\tau_p} + G(x) = 0, \quad (2.12)$$

where p_{n0} is the equilibrium hole density, and τ_p is the lifetime of excess carriers. The solution of Eq. (2.12) under the boundary conditions

$$p(x)=p_{n0} \quad \text{at } x=\infty, \quad (2.13)$$

and

$$p(x)=0 \quad \text{at } x=w, \quad (2.14)$$

is given by

$$p(x) = p_{n0} - \left(p_{n0} + Ke^{-\alpha w}\right)e^{(w-x)/L_p} + Ke^{-\alpha x}, \quad (2.15)$$

where $L_p = \left(D_p\tau_p\right)^{1/2}$, $\alpha = \alpha(\lambda)$, and

$$K = \frac{\Phi_{ph}T_m(\lambda)}{D_p}\cdot\frac{(\alpha L_p)^2}{\alpha\left[1-(\alpha L_p)^2\right]}. \quad (2.16)$$

The diffusion current density at $x=w$ is thus obtained as

$$J_{diff} = -q\Phi_{ph}T_m(\lambda)\frac{\alpha L_p}{1+\alpha L_p}e^{-\alpha w} - qp_{n0}\frac{D_p}{L_p}. \quad (2.17)$$

The *emission photocurrent* can be estimated as

$$J_{emis} = -q\Phi_{ph}P_a\eta_{int}\eta_{col}, \tag{2.18}$$

where P_a is the metal absorbance, η_{int} is the internal quantum yield, and η_{col} is the collection efficiency, which accounts for electron scattering from the surfaces, phonons, and cold electrons. The internal quantum yield for this mechanism is defined as the probability that an excited electron will "escape" into the semiconductor. This yield follows Fowler's relation[11,12]

$$\eta_{int} \propto \frac{(h\nu - q\Phi_B)^2}{h\nu}, \tag{2.19}$$

where Φ_B is the Schottky barrier height. For UV Schottky photodiodes, the role of photoemission can be negligible, considering that the Fowler's relation is not satisfied for λ<500 nm and the defects induced photocurrent is higher than photoemission from the metal for visible radiation.

The total photocurrent under monochromatic illumination and reverse bias is, therefore, the sum of I_{drift} and I_{diff} and is given by

$$\begin{aligned} I_{T(ph)} &= A(J_{drift} + J_{diff}) \\ &= -q\Phi_{ph}T_m(\lambda)A[1 - e^{-\alpha w}/(1 + \alpha L_p)] - A(qp_{n0}D_p / L_p). \end{aligned} \tag{2.20}$$

From the above equation, the current responsivity of the Schottky photodiode may be estimated as

$$\Re_i = \frac{I_{T(ph)}}{P_{opt}} \cong \frac{A(J_{drift} + J_{diff})}{P_{opt}}. \tag{2.21}$$

Using the Eq. (2.21), the spectral responsivity of the Schottky photodiode based on undoped n-GaN grown on sapphire substrate using MOCVD method was calculated from its absorption coefficient spectrum.[6] The results of the calculations are compared to experimental measurements in Fig. 2.4. The lower UV/visible contrast obtained in the theoretical calculation is due to the fact that for the absorption coefficient deduced from transmission measurement in our case is lager than the real one by limitation of the measurement at long wavelength (λ>375 nm).

As shown in the Fig. 2.4, the long diffusion length is useful to improve the spectral response. The diffusion length is proportional to the square root of the lifetime and the mobility of minority

carriers, i.e., it depends on the crystalline quality of the epitaxial layer. In the ideal case, low doping levels are advisable to achieve high responsivity (due to the larger depletion region) and a sharp cutoff. The high mobility values would result in low series resistance and long diffusion length, so that the epitaxial layer should be thin (<0.5 μm) to optimize the UV/visible contrast. The low mobility in state-of-the-art n-$Al_xGa_{1-x}N$ due to the high density of defects, increases the series resistance, and reduces the diffusion length, which determines the responsivity value.

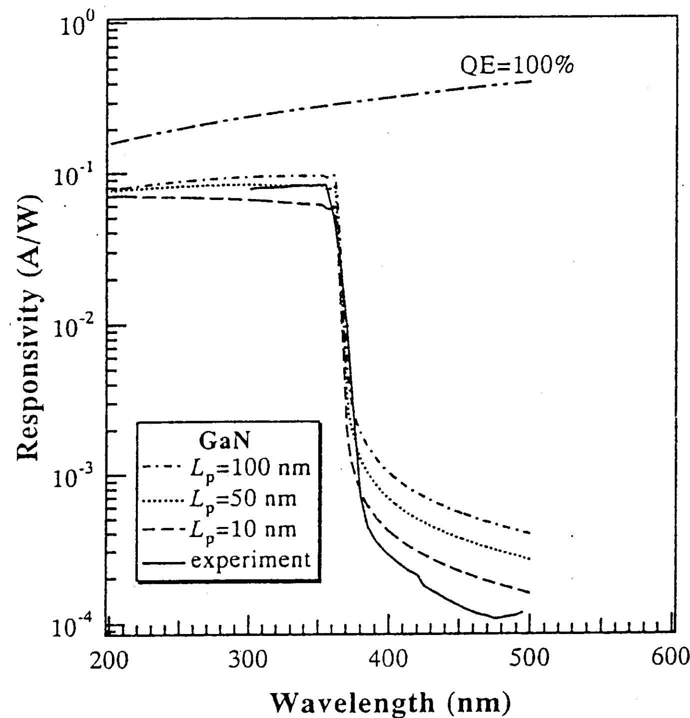

Fig. 2.4. Comparison of the experimental spectral responsivity of Au/n-GaN Schottky photodiodes with theoretical estimation assumed L_p=100, 50, and 10 nm , respectively. The responsivities corresponding to ideal quantum efficiency (QE=100%) is also shown.

In order to achieve high performance Schottky photodiodes on n-$Al_xGa_{1-x}N$ epitaxial layers, a moderate n-type doping level is recommended to improve the mobility, so that the series resistance decreases (larger bandwidth) and the diffusion length increases (higher responsivity). This doping level is even more important for higher Al contents, given the difficulty to achieve good ohmic contacts. The use of thick $Al_xGa_{1-x}N$ layers (>1μm) is preferable in this case, since the reduction in the dislocation density for thicker layers results in lower leakage currents and larger diffusion lengths (higher responsivity). Being the responsivity diffusion-limited, the increase of the layer

thickness does not degrade the UV/visible contrast.

2.2.3 Metal-semiconductor-metal photodetectors

The MSM structure can employ either back-to-back Schottky contacts (photovoltaic operation), or back-to-back ohmic contacts (photo-conductive operation). In general, the MSM photodetector (MSM-PD) is referred to as the photovoltaic one and ascribed to one kind of metal-semiconductor photodetectors. Because it employs the Schottky contact, the key advantage of Schottky barrier diode is remained, i.e., it is a majority carrier device and so does not suffer from speed delays arising minority carrier lifetime issue. The simple planar structure of MSM-PD results in two important features: (i) ultralow intrinsic capacitance; and (ii) simplicity in processing and fabrication, and processing compatibility with conventional FET-based electronics. These features are essential for building high-speed, high-sensitivity, wide-bandwidth optoelectronic receivers. For the application on the wide-bandgap GaN-based materials, it is easy to achieve high-quality Schottky contacts using the metals such as Pt, Pd, Ni, and Au ect..[13-17] In addition, the MSM approach avoids the difficult in obtaining high *p*-type doping and good ohmic contact on *p*-type GaN which are necessary for *p-i-n* diodes.

The MSM-PD consists of a layer of uniformly doped semiconductor material on which two Schottky barrier contacts are deposited.[18] The metal Schottky contacts are arranged to form two interdigitated fingers as shown in Fig. 2.3. Typically, the device is biased such that one of the two contacts is grounded while the other is reverse biased. At sufficiently high bias and small enough contact separation, the depletion regions beneath the Schottky gates can be connected. The applied bias at which the depletion regions touch is called the reach-through voltage, V_{RT}. The voltage at which the whole region between contacts is depleted is *reach-through voltage* (V_{rt}). Further increase of bias extends the depletion region toward the anode. The voltage at which the electric field at the anode reaches zero is termed *flat-band voltage* (V_{fb}). Further application of reverse bias acts to increase the electric field magnitude within the depletion region until avalanche breakdown is reached.

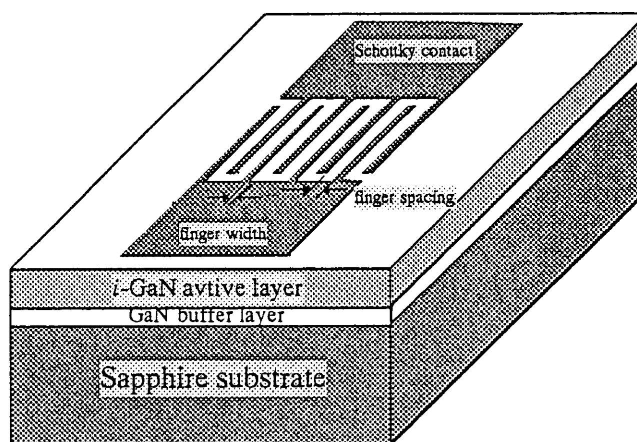

Fig. 2.5. Schematic drawing of a metal-semiconductor-metal interdigitated photodetector.

When the incident light falls on the top surface of the MSM structure, the light is absorbed within the underlying semiconductor at a depth depending upon its wavelength and the absorption coefficient of the material. The absorbed light produces electron-hole pairs. The application of a bias to the metallic fingers creates an electric field within the underlying semiconductor that sweeps the photogenerated carriers out of the depletion region. The speed and collection efficiency of the device varies depending upon the magnitude of the applied bias, the finger separation and the average depth at which the photogenerated carriers are produced.

The energy band diagram of a MSM-PD, consisting of two back-to-back Schottky contacts, is shown in Fig. 2.5. Increase of the applied bias increases the depletion region at the cathode as most of the voltages dropped across this reverse biased junction. The total photocurrent density is the sum of the current densities at the cathode, which is reverse biased by V_1, and the anode , which is forward biased by V_2 and is

$$J_{T(ph)} = J_{0+} + J_{L-}, \tag{2.22}$$

where J_{0+} (J_{L-}) is the current density at the metal-semiconductor junction of the cathode (anode) on the semiconductor side. Voltage and current definitions and directions are shown in Fig. 2.6.

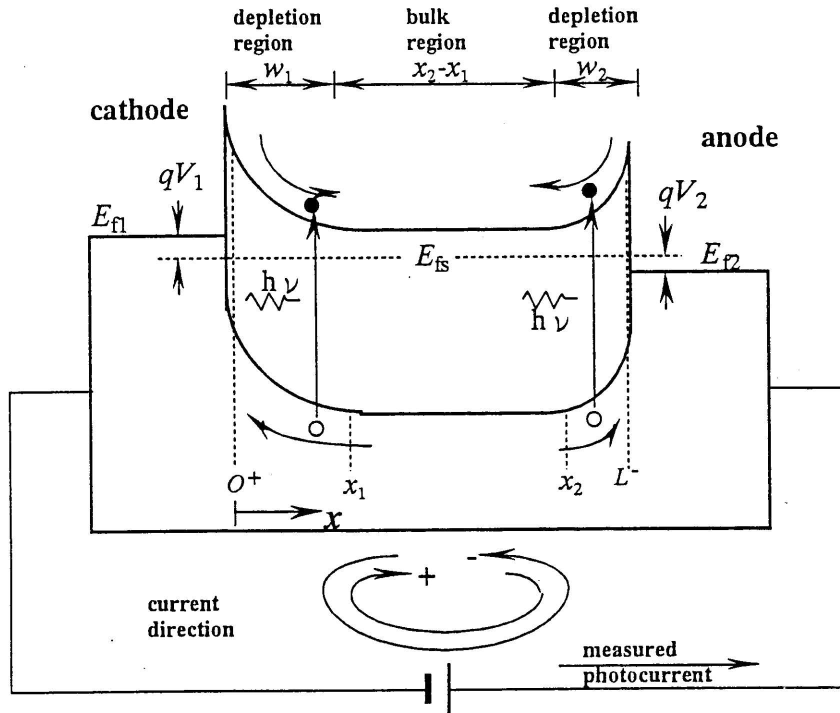

Fig. 2.6. Energy band diagram of a MSM photodiode under applied bias voltage.

Assuming that the optically generated carriers are in transit in the depletion region for a duration of much less than the recombination lifetime and further assuming that light response dominates the dark current flow, carrier recombination can be neglected and the continuity equation in the depletion region can be expressed as

$$-\frac{1}{q}\frac{\partial J_{T(ph)}}{\partial x}+G=0, \tag{2.23}$$

where q is the electron charge and G is the carrier generation rate. Integrating the above results in

$$J_{0+}=J_{x1}-qGw_1, \tag{2.24}$$

$$J_{L-}=J_{x2}+qGw_2, \tag{2.25}$$

where w_1 (w_2) represents the depletion region width of the cathode (anode) and J_{x1} and J_{x2} are currents at depletion edges of , respectively, the cathode and anode. Considering the background n doping of the active layer and the built-in barrier for electron motion at the contacts, these currents are due primarily to diffusion of minority carriers, holes, toward, respectively, the cathode and anode and are also effected by recombination with electrons accumulated in the concave shape of the conduction band. Contributions from thermionic emission of carriers from contacts to these

currents are neglected as light response is several orders of magnitude higher than dark current.

To determine J_{x1} and J_{x2} one can determine the minority carrier concentration in the undepleted region from the diffusion equation

$$D_p \frac{d^2 \delta p}{dx^2} - \frac{\delta p}{\tau_p} + G = 0, \tag{2.26}$$

where D_p is the diffusion coefficient, τ_p is the lifetime, and δp is the excess hole concentration. Because of the large electric field at cathode, it can be assumed that there are no holes at the edge of its depletion region , or

$$\delta p = -p_{n0} \quad \text{at} \quad x = x_1, \tag{2.27}$$

where p_{n0} is the equilibrium hole concentration .

The boundary condition at the anode is not the same as at the cathode because of asymmetry of the electric field distribution. We write this condition in terms of current continuity, expecting it to be dependent on generation rate is, as

$$-qD_p \frac{d\delta p}{dx} = qGf \quad \text{at} \quad x = x_2 \tag{2.28}$$

where f is a function of applied bias and light intensity and is in units of length. This condition could also be written in terms of excess carrier concentration and the velocity of carrier extraction, or transport V_t, as

$$-qD_p \frac{d\delta p}{dx} = q\delta p V_t \tag{2.29}$$

If V_t is of order of the diffusion velocity D_p/L_p and $\delta p = G\tau_p$, Eq. (2.28) equals qGL_p. This means that the two definitions are identical, allowing f to be interpreted as the effective diffusion length.

Solving Eq. (2.25) with these boundary conditions results in

$$\delta p(x) = K_1 \exp(x/L_p) + K_2 \exp\left(-x/L_p\right) + \frac{L_p^2}{D_p} G, \tag{2.30}$$

where K_1 and K_2 are given by

$$K_1 = \frac{-(p_{n0} + G\tau_p)\exp(-x_2/L_p) + \frac{L_p Gf}{D_p}\exp(-x_1/L_p)}{2\cosh\left(\frac{x_2 - x_1}{L_p}\right)}, \quad (2.31)$$

$$K_2 = \frac{-(p_{n0} + G\tau_p)\exp(x_2/L_p) + \frac{L_p Gf}{D_p}\exp(x_1/L_p)}{2\cosh\left(\frac{x_2 - x_1}{L_p}\right)}, \quad (2.32)$$

where x_2-x_1 is the width of the undepleted region.

Differentiating Eq. (2.30) and evaluating it at x_1 leads to an expression for diffusion current density:

$$J_{x1} = -qD_p \frac{\partial \delta p}{\partial x}\Big|_{x=x1}$$

$$= \left(-\frac{qD_p}{L_p}\right)\left[\frac{(G\tau_p + p_{n0})\sinh\left(\frac{x_2 - x_1}{L_p}\right) - \frac{L_p Gf}{D_p}}{\cosh\left(\frac{x_2 - x_1}{L_p}\right)}\right] \quad (2.33)$$

The total photocurrent density was found form Eqs. (2.22), (2.24), and (2.25) to be

$$J_{T(ph)} = J_{x1} + J_{x2} - qG(w_1 - w_2) \quad (2.34)$$

where the current density J_{x2} is given by the boundary condition described in Eq. (2.28), i.e., $J_{x2}=qGf$. Neglecting p_0 and substituting into Eq. (2.34) from Eqs. (2.28) and (2.33), the photocurrent of MSM-PD is then obtained as

$$J_{T(ph)} = -qG(w_1 - w_2) - qGL_p\tanh\left(\frac{x_2 - x_1}{L_p}\right) + qGf\,\mathrm{sec}h\left(\frac{x_2 - x_1}{L_p}\right) + qGf \ . \quad (2.35)$$

The first term in Eq. (2.35) is due to the electron-hole pairs that are generated in the depletion regions of the cathode and anode. The other terms describe the contribution of the holes generated in the undepleted region (x_2-x_1) between the cathode and anode. The middle two terms are due to

the carriers generated in the bulk and extracted at the end of the cathode depletion region. The last terms is the current that is due to the extraction of holes at anode end and has a sign opposite the first term. To demonstrate the generality of Eq. (2.35), it is discussed in several special cases.

A. Bias values below reach through

For values of the applied bias such that the undepleted bulk region is much larger than the diffusion length, the approximations $tanh[(x_2-x_1)/L_p]=1$ and $csch[(x_2-x_1)/L_p]=0$ reduce Eq.(2.35) to

$$J_{T(ph)} = -qG(w_1 + L_p) + qG(w_2 + f)$$

$$\text{for } x_2-x_1 >> L_p. \qquad (2.36)$$

Equation (2.30) clearly shows that carriers generated in the cathode depletion region and holes within a diffusion length of its edge produce the cathode current whereas holes generated in the anode depletion region and within a distance f of its edge comprise the anode current. Parameter f thus shows the average distance that holes diffuse toward the anode and are then swept by the electric field and collected. For this reason f can be termed the effective anode diffusion length. Parameters L_p and f are not generally equal since the electric field at the cathode and anode depletion region edge differ because of a much large potential drop across the cathode. As mentioned above, this formalism can be replaced by writing the current at anode depletion edge in term of carrier extraction velocity and by arguing that this velocity is different from that of cathode; but as all variables in Eqs. (2.35) and (2.36) have units of length, its present form is more descriptive.

For small values of voltage, however, equal numbers of holes can diffuse to the anode and cathode and the device become almost symmetrical, that is, f equals L_p, which reduces Eq. (2.35) to the simpler form of

$$J_{T(ph)} = -qG(w_1 - w_2) \quad \text{for small } V_b, \qquad (2.37)$$

The physical meaning of Eq. (2.37) is straightforward, but it is noteworthy that it becomes zero if no bias is applied.

B. Bias value close to reach-through

For high speed devices, the undepleted region is smaller than a diffusion length. Since application of bias further reduces this distance, Eq. (2.35) should be modified for for x_2-x_1<<L_p, by setting $\tanh[(x_2-x_1)/L_p]=(x_2-x_1)/L_p$ and $\text{sech}[x_2-x_1/L_p]=1$ to get

$$J_{T(ph)} = -qG(w_1 - w_2) - qG(x_2 - x_1) + 2qGf \quad \text{for } x_2\text{-}x_1 << L_p. \tag{2.38}$$

Three special cases of Eq. (2.38) are of interest. (I) If all the holes are collected at the cathode , f=0 and Eq. (2.38) indicates that all the carriers generated in the undepleted region will diffuse toward the cathode and are subsequently collected. this would overestimate the total current of the MSM-PD. (II) If half of the carriers generated in the bulk are collected at the anode and other half at the cathode , then $f=(x_2-x_1)/2$ and Eq. (2.38) reduces to Eq. (2.37), meaning that the total current is simply the difference of the carriers collected at the cathode and anode depletion regions. (III) The maximum value that f can assume is (x_2-x_1), corresponding to the case when all the carriers generated in the bulk diffuse to the anode. In this case Eq. (2.38) becomes

$$J_{T(ph)} = -qG(w_1 - w_2) - qG(x_2 - x_1) \tag{2.39}$$

This underestimates the total hole current but allows for the fact that not all the electrons generated in the depletion regions are collected as indicated by the first term of Eq. (2.39).

C. Bias values above reach-through

When the depletion regions between the cathode and anode meet, the length of the undpleted region is zero and , from Eq. (2.38) or Eq. (2.39), the photocurrent density is given by

$$J_{T(ph)} = -qG(w_1 - w_2). \tag{2.40}$$

For higher values of bias, the depletion region of the cathode impinges on the anode until the electric field at the anode becomes zero. For voltages higher than this flat-band voltage, the detector current is characterized by

$$J_{T(ph)} = -qGL, \tag{2.41}$$

where L is the distance between electrodes. It is expected that, for voltages higher than flat-band voltage but before breakdown, the current remains constant.

From the above discussion on Schottky barrier and MSM structure photodiodes, we get to know that the optical parameter of interest is the absorption coefficient, $\alpha(\lambda)$. The electrical parameters of interest are minority carrier diffusivity, D, and diffusion length, L. In photodetector, the excessive minority carriers, collected by an internal electric field in the depletion region, contribute to an electric current (generated due to radiation absorption) and, therefore, to a device photoresponse. the longer the minority carrier diffusion length, the larger amount of minority carriers able to reach the depletion region, and, hence, the better photodetector performance.

2. 3 CHARACTERISTICS and PARAMETERS

The main parameters of semiconductor photodetectors are the following.

(1) *Optical area* A_o

Optical area of a responsive element A_o is an area of the element generating photocurrent equal to the photocurrent of the detector with sensitivity uniform on the area and equal to the maximal local sensitivity of our responsive element. Obviously A_o is less than or equal to the electrical area of the illuminated surface of the responsive element A_e. The ordinary values of A_e are 0.1~100 mm^2.

(2) *Operation voltage* V_{op} .

Junction photodetectors can be used in zero-bias mode and in reverse-bias mode of photovoltaic detector operation. The operation voltage must be lower than the breakdown voltage V_{BR}, i.e. the maximum reverse voltage that can safely be applied to the photodiode before a breakdown occurs at the junction. An empirical expression was forwarded by Sze and Gibbons for the breakdown voltage of abrupt p -n junction and Schottky barrier diodes in Ge, Si, GaAs, and GaP:[19]

$$V_{BR} = 60\left(\frac{E_g}{1.1}\right)^{3/2}\left(\frac{N_B}{10^{16}}\right)^{-3/4}, \tag{2.42}$$

where E_g is the band gap in eV and N_B is the background doping in cm^{-3}. It has, however, been known that the Sze–Gibbons formula is generally not applicable in many wide band-gap materials, such as SiC and diamond. A more elaborate empirical relation is presented by Trivedi and Shenai[20] in terms of material parameters other than E_g alone, which is expressed as

$$V_{BR} = \left[2K(qN_B/\varepsilon_s)^3\right]^{-1/4}$$

$$K = 9\times10^{-38}\frac{A(216)^m}{b^{0.85}E_g^{15}} \tag{2.43}$$

where A, b, and m are the average impact ionization coefficients for electrons(n) or holes(p), and ε_s is the semiconductor permittivity. The value of A, b, and m for each material is tabulated in Table 2.1.

TABLE 2.1. Average ionization parameters.

Material	A (cm^{-1})	b (V/cm)	m	K (cm^6/V^7)
Si	1.07×10^6	1.65×10^6	1	1.9×10^{-35}
GaAs	2.24×10^5	6.343×10^5	1.79	1.8×10^{-35}
GaP	4.0×10^5	1.18×10^6	2	5.5×10^{-38}
6H-SiC	3.42×10^6	1.335×10^7	1	4.8×10^{-42}
GaN	8.85×10^6	2.6×10^7	1	9.1×10^{-43}

The breakdown voltages as a function of background doping for Si, GaP, 6H-SiC, and GaN are shown in Fig. 2.7.

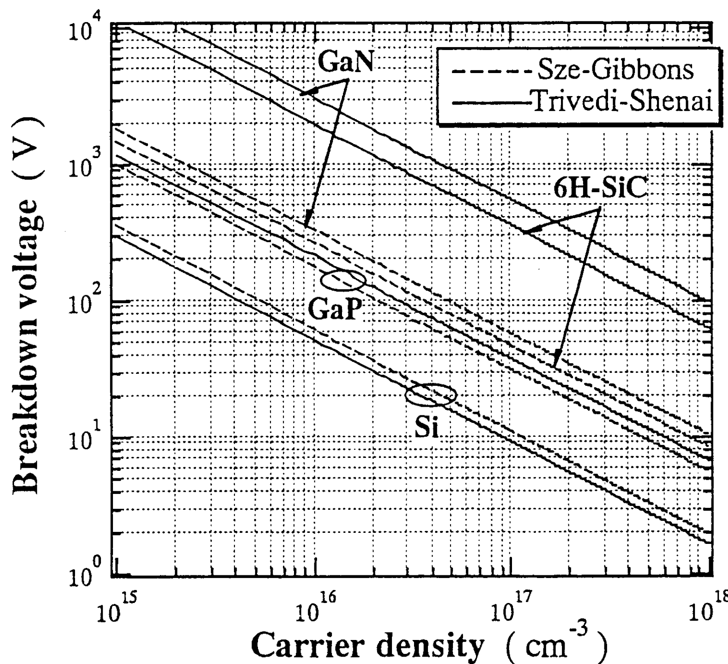

Fig. 2.7. The calculated breakdown voltages for Si, GaP, 6H-SiC, and GaN. Predictions from the Sze–Gibbons relation are plotted as dashed lines.

(3) ***Photocurrent–radiant flux characteristic*** $I_{ph}(\Phi)$.

The radiant flux density F_p dependence of photocurrent density J_p must be linear over a wide range of the flux density $J_p(F_p) = \kappa F_p$.

The coefficient κ is called the *current responsivity* $\Re_i$ (A/W); this parameter is obtained as the short-circuit light current density (A/cm^2) divided by the radiant flux density of the light (W/cm^2). At the same time the coefficient κ is called the *quantum efficiency* (electrons/photon) when the flux density refers to equal amounts of incident photons; this parameter is the number of electrons or holes that can be detected as a photocurrent divided by the number of incident photons.

In a well-designed photodetector, nearly all photons penetrating the semiconductor are absorbed and they result in carrier generation followed by efficient carrier collection. If all of these processes are done to perfection, the internal quantum efficiency η_0 for this photodetector is nearly unity. An expression for η_0 is

$$\eta_0 = \left(I_p / q\right) / \left(P_{opt} / h\nu\right), \tag{2.44}$$

where I_p is the photogenerated current by the absorption of incident optical power P_{opt} at a wavelength λ(corresponding to a photon energy $h\nu$). However, under usual circumstances, the actual quantum efficiency which also includes the reflections and other external losses, is lower than the internal quantum efficiency η_0. This is called the external quantum efficiency η_{ext}. The quantum efficiency depends on internal quantum efficiency η_0, loss coefficient γ and reflectivity of surface R:

$$\eta_{ext} = \eta_0 (1 - \gamma)(1 - R). \tag{2.45}$$

The loss coefficient γ is determined by photocarrier recombination in the bulk and on the surface of a semiconductor and by diffusion (or thermionic emission) of charge carrier against the built-in electric field; the value of the last type of loss decreases with increasing carrier concentration.

The photoconductive gain "g" is another parameter of a detector (photo-conductive variety) and is defined as the number of carriers passing through the contact per each generated electron–hole pair. This gain describes how efficiently the generated electron–hole pairs are used to create electric current. The spectral current responsivity of a photodetector can then be expressed as:

$$\Re_i = \frac{\lambda q}{hc}\eta_{ext} g = \frac{q}{h\nu}\eta_{ext} g, \qquad (2.46)$$

where λ is the wavelength, h is Planck's constant, c is the light velocity, q is the electron charge, g is the photoconductive current gain, and ν is frequency of the light. The actual measured variable is the responsivity $\Re$. Thus, it is clear that one cannot decouple the actual quantum efficiency from any internal gain present in the device.

Sometimes the term voltage responsivity $\Re_v$ (V/W) is used; this parameter is obtained as the photoresponse voltage divided by the radiant flux, but in this case it is necessary to indicate not only wavelengths but flux densities also.

(4) ***Dark current–voltage characteristic*** (I_d-V_b).

A fundamental characteristics of great importance in UV photodetector performance is the device dark current and UV photoresponse. Low dark current is very important for high-speed optical pulse detection. For photodetectors employed Schottky contacts, if the Schottky contact is poor, excess carriers are injected into the semiconductor over the Schottky barrier, and the response time is increased.

The low dark current drastically diminishes the current noise. That is also important in lowering the minimum detectable power, which is equal to the shot noise current and is shown as follows:

$$q \cdot \frac{\eta P_{min}}{h\nu} = \sqrt{2qI_d B}, \qquad (2.47)$$

where is the quantum efficiency, P_{min} is the minimum detectable power, h is Planck's constant, ν is the irradiated light frequency, and B is the bandwidth.

The dark current I_d in Schottky diodes based on wide-gap high-mobility semiconductors at low doping levels and small bias voltage is determined by thermionic emission[21]

$$\begin{aligned} I &= I_0 \exp(qV_b/nkT)[1-\exp(-qV_b/kT)] \\ &= AA^{**}T^2 \exp(-q\phi_B/kT)\{\exp(qV_b/nkT)[1-\exp(-qV_b/kT)]\}, \end{aligned} \qquad (2.48)$$

where q is the electron charge, A is the area, I_0 is the saturation current, k is the Boltzmann

constant, T is the operating temperature (K), n is the ideality factor, A^{**} is the Richardson constant ϕ_B is the barrier height, and V_b is the applied bias voltage. This dependence is used for the calculation of the shunt resistance of a photodiode which is the voltage-to-current ratio in the vicinity of 0 V, $R_0=nkT/(qI_0)$, dark resistance and dark current I_d at the operation voltage. These parameters deteriorate markedly with decreasing contact (diffusion) potential (and semiconductor bandgap) and with increasing carrier concentration.

At higher concentrations and bias voltages V_b, I_d is determined by thermofield emission[22]

$$I_d = I_s \exp\left\{\frac{qV_b}{E_{00}}\left[\frac{E_{00}}{kT} - \tanh\left(\frac{E_{00}}{kT}\right)\right]\right\},$$

$$I_s = AA^{**}T\frac{\sqrt{\pi E_{00}}}{k}\left[q(V_b - V_n) + \frac{q\phi_B}{\coth^2(E_{00}/kT)}\right]\exp\left[-\frac{q\phi_B}{E_{00}\coth(E_{00}/kT)}\right], \tag{2.49}$$

where V_n is the Fermi level energy in the semiconductor and E_{00} is the characteristic energy parameter

$$E_{00} = \frac{qh}{4\pi}\sqrt{\frac{N_D}{m^* \varepsilon_r \varepsilon_0}}, \tag{2.50}$$

where h is Planck's constant, m^* the carrier effective mass, N_D the donor density, and ε_r, ε_0 are the dielectric constants of the semiconductor and vacuum, respectively.

Consideration of the MSM-PD as two back-to-back n-type Schottky contacts dictates that the anode contact will be forward biased and the cathode contact reverse biased under an external applied bias voltage. Assuming that the two contacts operate as thermionic-emission-limited diodes, the dark current-voltage characteristics of the MSM-PD can be described as the following.[23]

(I) Bias voltage $V_b<V_{RT}$

For low biases such that the sum of the depletion widths w_1 and w_2 are smaller than the finger spacing L, the charge distribution in an MSM-PD is shown in Fig. 2.8.(a) for an n-type semiconductor with doping density N_d. The corresponding electric field and the potential

distribution are shown in Figs. 2.8 (b) and (c).

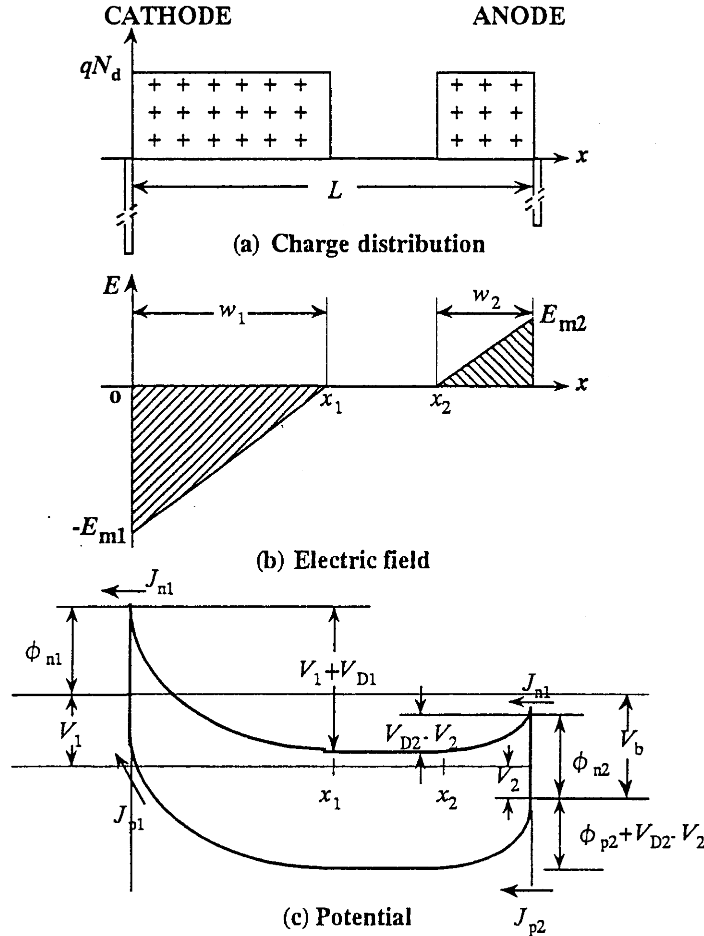

Fig. 2.8. The charge distribution, electric field, and potential profile of an MSM structure under bias voltage.

In this case, the total dark current density may be expressed as

$$J_d = J_{n1} + J_{p1} = J_{ns} e^{q\Delta\phi_{n1}/kT}\left(1 - e^{-qV_1/kT}\right) + \frac{qD_p p_{no} \tanh\left[(w_2 - w_1)/L_p\right]}{L_p} \cdot \left[1 - \exp(-qV_1/kT)\right] + \frac{J_{ps}\exp(-qV_{D2}/kT)}{\cosh\left[(w_2 - w_1)/L_p\right]} \cdot \left[\exp(qV_2/kT) - 1\right], \quad (2.51)$$

with $J_{ns} = A_n^* T^2 \exp(-q\phi_{n1}/kT)$, (2.52)

$J_{ps} = A_p^* T^2 \exp(-q\phi_{p2}/kT)$, (2.53)

where J_{ns} (J_{ps}) is the saturation current densities of electron (hole), ϕ_{n1} (ϕ_{p2}) is the Schottky barrier heights for electrons (holes), A_n^*(A_p^*) is the effective Richardson's constant for electron (hole) emission, V_{D2} the built-in potential at the anode contact, and $\Delta\phi_{n1}$ the image-force lowering of ϕ_{n1}.

(II) $V_{RT}<V_b<V_F$

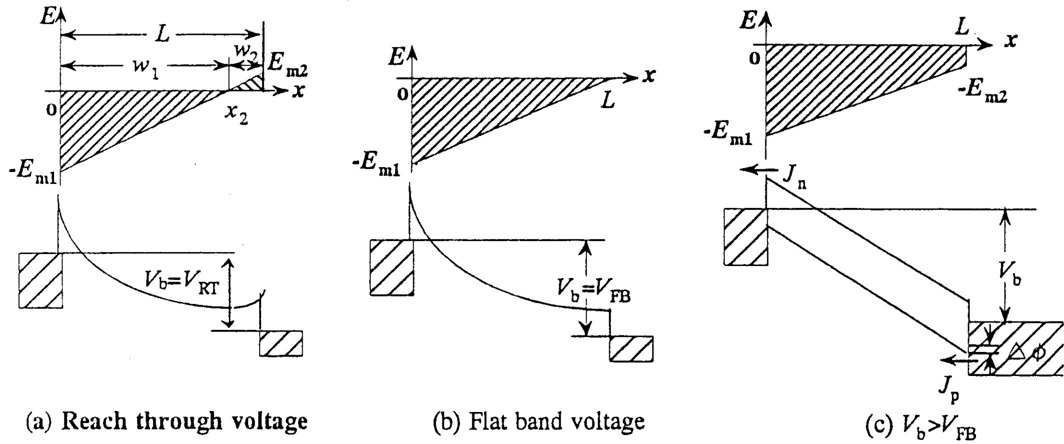

(a) **Reach through voltage** (b) Flat band voltage (c) $V_b>V_{FB}$

Fig. 2.9. (a) Case of reach-through; (b) Case of flat-band; (c) Case for bias voltage $V_b>V_{FB}$, $\Delta\phi$ is the image-force lowering of ϕ_{p2}.

In the case of $V_{RT}<V_b<V_{FB}$, the electric field and potential profile are illustrated in Fig. 2.9.(a). The expression of J_d is given by

$$J_d = J_{ns}\exp(q\Delta\phi_{n1}/kT) + J_{ps}\left[\exp\left(-\frac{q}{kT}\cdot\frac{(V_b - V_{FB})^2}{(V_{FB} - \Delta V_D)}\right) - \exp(-qV_{D2}/kT\right], \tag{2.54}$$

$$V_{FB} = \frac{qN_d}{2\varepsilon_r\varepsilon_0}L^2 - \Delta V_D, \tag{2.55}$$

$$\Delta V_D = V_{D1} - V_{D2}, \tag{2.56}$$

where V_{FB} is the flat-band voltage, V_{D1} is the built-in potential at the cathode contact. For a symmetrical MSM-PD, i.e., $\Delta V_D = 0$, equation (2.49) reduces to

$$V_{FB} = qN_dL^2/(2\varepsilon_r\varepsilon_0). \tag{2.57}$$

(III) $V_b>V_{FB}$

As shown in Fig. 2.9 (C), in this situation the total dark current density is

$$J_d = J_{ns}\exp(q\Delta\phi_{n1}/kT) + J_{ps}\exp(q\Delta\phi_{p2}/kT). \tag{2.58}$$

The dark current that flows under an applied voltage will in general be determined by that region which absorbs the greatest fraction of the voltage, i.e., by the region which limits the current to greatest degree. For the n-GaN based MSM-PD, the electron barrier height ϕ_{n1} (about 1eV) is usually smaller than the hole barrier height ϕ_{p2} (is estimated as E_g^{GaN} -ϕ_{n1}=2.4 eV), that is , the hole current will be always smaller than the electron current. So that the total dark current can be

essentially given by the first term of Eq. (2.51). In other words, if the hole barrier is high, then the electron current from cathode contact will account for the entire behavior which is essentially the same as a simple Schottky diode with anode contact replaced by an ohmic, non-injecting contact.

(5) ***Detectivity and noise parameters.***

Detectors and noise are synonymous in that the minimum detectable radiation power is determined by the noise floor of the detector. The noise sources can be categorized into two groups, one being internal to the detector (resulting from one or ore sources) and the other being the radiation noise due to the environment (background radiation), both of which are very important. In the limit of the minimum radiant power that is to be detected, all detectors experience a noise wall. The potential sources of noise are fluctuations in the detector itself, in the radiant energy to which the detector responds, or in the electronic system accompanying the detector. Usually, the signal fluctuations and background fluctuations are considered to be responsible for the radiant noise. However, under most operating conditions in the UV, the background fluctuation is minimal, and the radiant noise is dominated by the signal fluctuations. In a photodetector, the free carriers always exhibit random thermal motion, and because of this, there occurs a fluctuation in the velocity of these carriers, which leads to internal noise. The fluctuations in the density of free carriers due to randomness in the rates of thermal generation and recombination (G-R) also contribute to the internal noise. There can be four different types of internal noise in a photoconductor. These are Johnson noise, 1/f noise, G–R noise (shot noise), and preamplifier noise. All of these noise components are expressed in terms of current across the detector terminals.

The *noise equivalent power* (NEP) is the amount of optical-signal equivalent to the noise level of a device. It is the root-mean-square (rms) value of the first harmonic of incident modulated radiant flux $P(\omega)$ with the given spectrum which creates the rms value of the first harmonic of the photoresponse current I_p (or photoresponse voltage V_p) which is equal in the value to the rms value of noise current I_n (or voltage V_n) at the given modulator frequency. If one expresses the above

description in formula, it will be

$$P(\omega) = P_{opt}\left(1 + me^{j\omega t}\right), \tag{2.59}$$

$$\text{NEP=rms optical power } (P_{opt})_{min} \text{ with S/N=1}, \tag{2.60}$$

Where P_{opt} is the average optical signal power, m is the modulation index, ω is the modulation frequency, and S/N is the photoresponse singal-to-noise ratio.

Unit frequency bandwidth noise equivalent power, UFB-NEP=I_n / I_pf $^{1/2}$ (W Hz $^{-1/2}$), is the noise equivalent power normalized for frequency bandwidth, and *specific noise equivalent power* NEP* (W Hz$^{-1/2}$ cm^{-1}) is the noise equivalent power normalized for frequency bandwidth and detector active area. Detectivity D (W^{1}Hz$^{1/2}$) is the reciprocal of UFB-NEP value and specific detectivity D* (W^{-1}Hz$^{1/2}$cm) is the reciprocal of NEP* value.

If the current gain *g for* the photocurrent and the noise current is the same, then the current noise resulting from the *G–R* process is

$$I_n = qg\left\{2A_e\Delta\nu\left[t(G+R)\right]\right\}^{1/2}, \tag{2.61}$$

where $\Delta\nu$ is the bandwidth in terms of frequency, G and R are the generation and recombination rates, respectively, t is the thickness of the detector, and A_e is the electrical area of the detector. The generation rate G is a combination of the optical generation rate G_{op} and the thermal generation rate G_{th}: $G=G_{op}+G_{th}$.

If A_o is the optical area of the detector, then the normalized signal-to-noise performance of this detector can be determined by the specific detectivity, D*. The specific detectivity represents the signal to noise ratio when normalized to a standard size. The D* detectivity is given by

$$D^* = \frac{\Re_i (A_o \Delta\nu)^{1/2}}{I_n}, \tag{2.62}$$

Eqs. (2.60)–(2.61) yield

$$D^* = \frac{\eta\lambda}{hc}\left\{\frac{A_o}{2[t(G+R)]A_e}\right\}^{1/2}, \tag{2.63}$$

where h is Planck's constant, c the speed of light. The specific detectivity increases with increasing

quantum efficiency and wavelength of incident light and decreasing dark current.

The optical area A_o and electrical area A_e of a photodetector are generally different from having to make it-contact to the semiconductor which blocks the radiation from reaching the semiconductor. An examination of Eq. (2.62) indicates that, for a given wavelength λ, and operating temperature T, the highest performance of the photodetector can be obtained by maximizing $\eta/[t(G+R)]^{1/2}$ the recombination process takes place in a region of the device (for example, at the contacts in sweep out photoconductors (PCs) or in the neutral reconverted regions of the diode types) where the photoelectric gain is marginally small, the effect of fluctuating recombination is quite negligible. Because of this, the noise can be low by as much as 2.5 times and the detectivity will be high by the same proportion. The generation process with its associated fluctuation cannot, however, be avoided by any means. The generation and recombination rates are equal at equilibrium. Hence assuming A_o=A_e, we get

$$D^{*} = \frac{\lambda\eta}{2hc}\left(\frac{1}{Gt}\right)^{1/2}, \tag{2.64}$$

In a photodetector the optical generation G_{op} may be due to the signal or thermal background radiation. If, for this photodetector, G_{th} is at a level where $G_{th} \ll G_{op}$, then the NEP may be defined by

$$NEP = \frac{(A\Delta v)^{1/2}}{D^{*}}, \tag{2.65}$$

where A is the area of the device.

In background limited detectors, meaning when the background radiation noise is dominant, the NEP is given by

$$NEP = hv\left(\frac{2A\Phi\Delta v}{\eta}\right)^{1/2}, \tag{2.66}$$

where Φ is the total background radiation impinging on the detector (expressed as background radiation flux density (photons/s-cm^2)) and the specific detectivity in a photovoltaic detector

(operation at zero bias) is given by

$$D^* = \Re_i\left[(4kT/R_0A) + 2q^2\eta_{ext}\Phi\right]^{-1/2}, \quad (2.67)$$

where R_0 is the zero-bias resistance of the detector. In cases where the total background radiation is very small compared to the noise generated in the detector, the thermal noise limited detectivity is given by

$$D^* = \Re_i(R_0A/4kT)^{1/2}. \quad (2.68)$$

In cases where the detector is background limited, which solar blind detector seeks to avoid, the detectivity is given by

$$D^* = R_i\left(2q^2\eta_{ext}\Phi\right)^{-1/2}. \quad (2.69)$$

(6) ***Normalized transfer characteristic***

The normalized transfer characteristic is the time dependence of the detector parameters after a sudden change in light level. When the device is excited with rectangular light pulses, the time required for the output to rise from 0.1 to 0.9 of its final value is called the rise time t_r of the normalized transfer characteristic; the time required for the output to fall from 0.9 to 0.1 of its on-state value is called the decay time of the normalized inverse characteristic t_d. The cut-off frequency f_c is the frequency at which the photodiode output decreases by 3 dB (0.7) of the low-frequency response. In the special case of exponential transient response, the decay time and the rise time are related to the exponential time constant, τ, and to the device bandwidth, B, by the expressions

$$B = \frac{1}{2\pi\tau} = \frac{2.20}{2\pi\tau_d} = \frac{2.20}{2\pi\tau_r}, \quad (2.70)$$

It is very important to notice that reliable information about the device bandwidth can only be obtained from the photocurrent rise time if the excitation pulse is rectangular, with a rise time much shorter than t_r, and a pulse width much larger than t_r, so that photocurrent increases from zero to a steady-state value.

(7) ***Capacitance C***

The capacitance C is the major factor in determining the response speed of the photodiode. For Schottky photodiode,

$$C = A\left(\frac{q\varepsilon_r\varepsilon_0 N_d}{2}\right)^{1/2}\left(V_{bi} + V_r - \frac{kT}{q}\right)^{-1/2}, \tag{2.71}$$

where A is the Schottky contact area, N_d is the doping density, ε_0 is the dielectric constant of vacuum, ε_r is the relative effective dielectric constant of the semiconductor, V_{bi} is the built-in potential, and V_r is the bias voltage.

The time response of Schottky photodiode can be limited by capacitive effects, by carrier trapping, or by the saturation velocity of carriers in the semiconductor. All these phenomena reduce the responsivity at high frequencies. In GaN-based Schottky photodiodes, the linear dependence of the time constant on the load resistance ($\tau = \tau_0 + R_L C$, where τ_0 is the time constant at zero load) points to a RC_s-limited time response, where C_s is the sum of the diode internal capacitance (C) and the load capacitance (C_L), and R is the sum of the load resistance (R_L) and the series resistance of the device (R_s). For low load, the minimum time response is given by the product of R_s and C. The series resistance R_s is the resistance of the detector through which the photodiode current must flow, that is, the sum of resistances of semiconductor bulk and Ohmic contacts. Since the series resistance does not depend on bias, the device time response decreases proportionally to $(V_{bi}+V_r-kT/q)^{-1/2}$.

For diodes with the same geometry and polarization, C and R_S are proportional to $(N_d)^{1/2}$ and $(\mu_n N_d)^{-1}$ respectively, where μ_n is the electron mobility. Therefore, the bandwidth of these devices would be optimized by increasing $(\mu_n N_d)^{1/2}$. Under this assumption, Si-doping should improve the time response of Schottky photodiodes based on n-GaN, provided that mobility does not decrease drastically and Schottky barrier is not much lowered by tunnel transport.

For undoped and infinitely thick materials, the capacitance of planar interdigitated MSM-PD, using a theoretical model based on conformal mappings, is given by

$$C_0 = \frac{\varepsilon_0(1+\varepsilon_r)K}{K'}, \tag{2.72}$$

where C_0 is the capacitance per finger length, K and K' are elliptic integrals defined as

$$K = K(k) = \int_0^{\pi/2} \frac{d\phi}{\sqrt{1-k^2\sin^2\phi}},$$

$$K' = K(k'), \qquad k' = \sqrt{1-k^2},$$

$$k = \tan^2 \frac{\pi w}{4(s+w)}, \tag{2.73}$$

where w is the finger width and s is the finger spacing. The total detector capacitance is given by

$$C = C_0 A/(s+w), \tag{2.74}$$

where A is the detection area of detector. This indicates that for a given detector area and finger pitch (i.e., sum of the finger width and spacing) size, the smaller the finger width , the smaller the detector's capacitance. It should be noted that the capacitance of the interdigitated MSM-PD can be presented in a more simple form of :

$$C = \frac{A\varepsilon_0(1+\varepsilon_r)}{s+w} \cdot \frac{\pi}{4\ln\left(\frac{8}{\pi} + \frac{s}{w}\right)}, \tag{2.75}$$

The above equation is more suitable and efficient in analysis of the interdigitated MSM-PD geometry.

The time response, τ, of MSM-PDs is primarily limited either by the transit time of the optically generated cariers, t_{tr} , or by the device capacitance, C: The transit time can be estimated by:

$$\tau_{tr} = \frac{s\chi}{2\upsilon},$$

$$\frac{1}{\upsilon^4} = \frac{1}{2}\left(\frac{1}{\upsilon_e^4} + \frac{1}{\upsilon_h^4}\right). \tag{2.76}$$

where χ is carrier drift distance corrective coefficient, υ is carrier drift mean velocity υ_e and υ_h, are the electron and hole saturation velocity, respectively.

The RC -time constant of the equivalent circuit composed from the interdigitated MSM-PD capacitance C and diode load resistance R_L is given by:

$$\tau_{RC} = 2.2 R_L C. \tag{2.77}$$

The RC -time constant along with transit time limitations must be considered together to give a simple first order approximation to the overall response time of the MSM-PD:

$$\tau = \sqrt{\tau_{tr}^2 + \tau_{RC}^2}. \tag{2.78}$$

It is obvious from the above equations that for the MSM-PD with a fixed finger width and a given detection area, the minimum time response will take place under the condition $\tau_{tr} = \tau_{RC}$.

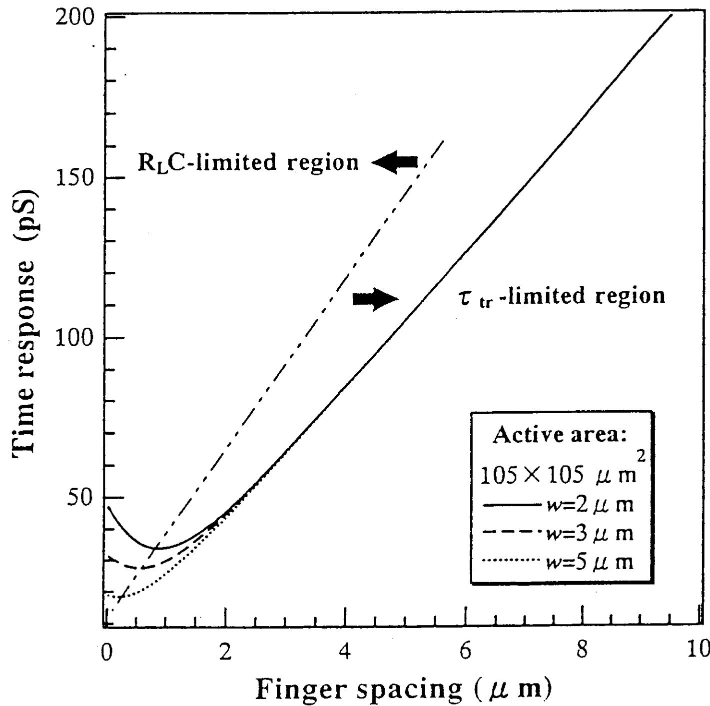

Fig. 2.10. Estimation of the time response of GaN MSM photodiodes as a function of finger spacing with the active area of 105×105 μ m^2.

Figure 2.10 demonstrates the calculated time response as a function of finger spacing for n-GaN MSM-PD with A=105× 105 μm^2 and w=2, 3, 5 μm. The other parameters employed in the calculation are R_L=50 Ω, χ=2, ε_r=9.5, υ_e=2.4×10^7 cm/s, υ_h=4×10^{6}cm/s.

(8) ***Responsivity–temperature characteristics*** $\Re$(T)

The quantum efficiency temperature coefficient η_T is the value $\eta_T=[(\eta_2-\eta_1)/(T_2-T_1)]\times100\%$ where η_1 and η_2 are the quantum efficiencies at the temperatures T_1 and T_2. With increasing temperature

the long-wavelength limit of the spectral sensitivity usually moves up in wavelength owing to decreasing semiconductor bandgap and the dark current increases exponentially. The temperature dependence of the quantum efficiency depends on the temperature dependence of the internal quantum yield, diffusion length of minority carriers and carrier recombination velocities in the semiconductor bulk or on its surface.

References

[1] B. Monemar, Phys. Rev. B **10**, 676 (1974).

[2] T. Ogino and M. Aoki, Jpn. J. Appl. Phys. **19**, 2395 (1980).

[3] M. Suzuki and T. Uenoyama, Jpn. J. Appl. Phys. **35**, 1420 (1996).

[4] G. D. Chen, M. Smith, J. Y. Lin, H. X. Jiang, S. H. Wei, M. A. Khan and C. J. Sun, Appl. Phys. Lett. **68**, 2784 (1996).

[5] For a detailed discussion, see for example, J. I. Pankove, *Optical Progress in semiconductor*, Dover Publication, Inc. New York (1975).

[6] G. Y. Zhao, H. Ishikawa, H. Jiang, T. Egawa, T. Jimbo, and M. Umeno, Jpn. J. Appl. Phys., Part 2 **38**, L993 (1999).

[7] S.S. Li, F.A. Lindholm and C.T. Wang, J. Appl. Phys. **43**, 4123 (1972).

[8] B.I. Reznikovand G.V. Tsarenkov, Sov.Phys.—Semicond. **25**, 1158 (1991).

[9] Yu.A. Goldberg, T.V. Lvova, O.A. Mezrin, S.I. Troshkov and B.V. Tsarenkov, Sov. Phys.Semiconduct. **24**, 1990 (1990).

[10] Yu.A. Goldberg, O.V. Konstantinov, E.A. Posse and B.V. Tsarenkov, Semiconductors **29**, 215 (1995).

[11] R.H. Fowler,Phys. Rev. **38**, 45 (1931).

[12] C.L. Anderson, C.R. Crowell and T.W. Kao, Solid-State Electron. **18**, 705 (1975).

[13] J. D. Guo, M. S. Feng, R. J. Guo, F. M. Pan, and C. Y. Chang, Appl. Phys. Lett. 67, 2657 (1995).

[14] L. Wang, M. I. Nathan, T-H. Lim, M. A. Khan, and Q. Chen, Appl. Phys. Lett. 68, 1267 (1996).

[15] Q. Z. Liu, L. S. Yu, S. S. Lau, F. Deng, and J. M. Redwing, J. Appl. Phys. 84, 881 (1998).

[16] L. S. Yu, D. J. Qiao, Q. J. Xing, S. S. Lau, K. S. Boutro, and J. M. Redwing, Appl. Phys.

Lett. **73**, 238 (1998).

[17] S. K. Noh and P. Bhattacharya, Appl. Phys. Lett. **78**, 3642 (2001).

[18] J. B. D. Soole and H. Schumacher, IEEE J. Quantum Electron. **27**,737 (1991).

[19]S. M. Sze and G. Gibbons, *Appl. Phys. Lett.* **8**, 111 (1965); S. M. Sze, *Physics of Semiconductor Devices* (Wiley, New York, 1981).

[20] M. Trivedi and K. Shenai, J. Appl. Phys., **85**, 6889 (1999).

[21] E. H. Rhoderick and R. H. Williams: *Metal-Semiconductor Contacts* (Clarendon, Oxford, 1988).

[22] F.A. Padovani and R. Stratton, Solid-State Electron. **9**, 695 (1966).

[23] S. M. Sze, D. J. Coleman, Jr., and A. Loya, Solid-State Electron. **14**, 1209 (1971).